Physical Biology

PAPER

From the volcano effect to banding: a minimal model for bacterial behavioral transitions near chemoattractant sources

Gregory Javens[1], Hossein Jashnsaz[2] and Steve Pressé[3,4]

1. Department of Mathematics and Statistics, CUNY Hunter College, New York, NY 10065 United States of America
2. Department of Physics, Indiana University—Purdue University Indianapolis (IUPUI), Indianapolis, IN 46202, United States of America
3. Department of Physics, Arizona State University, Tempe, AZ 85281, United States of America
4. School of Molecular Sciences, Arizona State University, Tempe, AZ 85281, United States of America   AQ1

E-mail: stevenpresse@gmail.com

Abstract

Sharp chemoattractant (CA) gradient variations near food sources may give rise to dramatic behavioral changes of bacteria neighboring these sources. For instance, marine bacteria exhibiting *run-reverse* motility are known to form distinct bands around patches (large sources) of chemoattractant such as nutrient-soaked beads while *run-and-tumble* bacteria have been predicted to exhibit a 'volcano effect' (spherical shell-shaped density) around a small (point) source of food. Here we provide the first minimal model of banding for *run-reverse* bacteria and show that, while banding and the volcano effect may appear superficially similar, they are different physical effects manifested under different source emission rate (and thus effective source size). More specifically, while the volcano effect is known to arise around point sources from a bacterium's temporal differentiation of signal (and corresponding finite integration time), this effect alone is insufficient to account for banding around larger patches as bacteria would otherwise cluster around the patch without forming bands at some fixed radial distance. In particular, our model demonstrates that banding emerges from the interplay of *run-reverse* motility and saturation of the bacterium's chemoreceptors to CA molecules and our model furthermore predicts that *run-reverse* bacteria susceptible to banding behavior should also exhibit a volcano effect around sources with smaller emission rates.
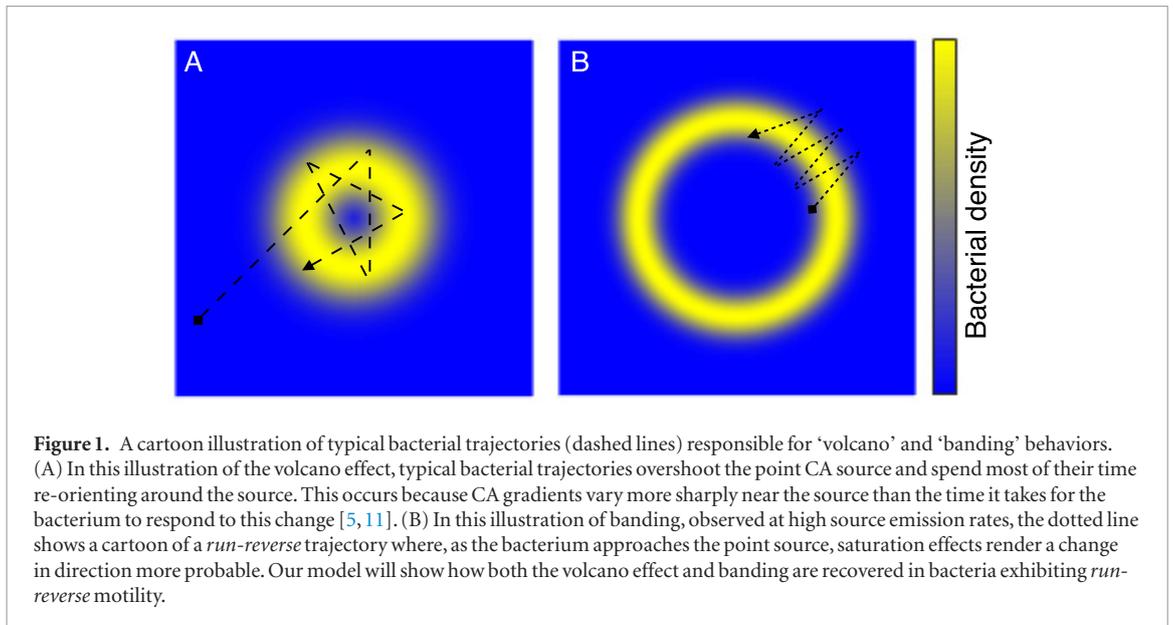
Introduction

Chemotaxis is the process by which bacteria swim toward chemoattractant (CA) or away from chemorepellant (CR) [1, 2]. Modeling bacterial dynamics near CA sources is relevant in describing how bacteria accumulate around and track CA sources [3–6] especially in active and turbulent flow [7]. While chemoattraction may be less important in helping predatory bacteria, such as *Bdellovibrio bacteriovorus* (*Bb*), locate individual prey [8], even *Bb* is attracted to larger prey patches that serve as CA sources [8].

Here we revisit the idea of chemoattraction toward point sources in an effort to reconcile two disparate bacterial behaviors near sources, banding and the volcano effect, described below. The general model we propose captures the broad range of bacterial dynamics, both (1) predicted and (2) observed, around point CA sources: (1) The predicted behavior we are interested in includes the volcano effect where bacteria form a shell of higher density around a point CA source as a result of individual bacteria consistently overshooting the peak in the CA concentration due to a delay in their chemotactic response [11]. (2) The observed behavior includes the formation of bands (of width, say, 20 μm and an average distance of order 40 μm away from bead surfaces [3]) by marine bacteria with *run-reverse* motility around CA loaded beads. An illustration of both effects, 'volcano' and 'banding', is given in figure 1.

Our goal here is to develop a minimal model of banding, directly motivated from more basic features of bacterial dynamics (such as bacterial saturation to signal, i.e. bacterial adaptation). By contrast to *run-and-tumble* bacterial motility which our model suggests cannot exhibit banding, we show that both the volcano effect and banding emerge from a single *run-reverse* bacterial motility model under different CA

Figure 1. A cartoon illustration of typical bacterial trajectories (dashed lines) responsible for 'volcano' and 'banding' behaviors. (A) In this illustration of the volcano effect, typical bacterial trajectories overshoot the point CA source and spend most of their time re-orienting around the source. This occurs because CA gradients vary more sharply near the source than the time it takes for the bacterium to respond to this change [5, 11]. (B) In this illustration of banding, observed at high source emission rates, the dotted line shows a cartoon of a *run-reverse* trajectory where, as the bacterium approaches the point source, saturation effects render a change in direction more probable. Our model will show how both the volcano effect and banding are recovered in bacteria exhibiting *run-reverse* motility.

point source emission rates where different model features are at play; see figure 1. For instance, we find that the volcano effect arises in *run-reverse* bacteria from temporal differentiation of signal and, as the emission rate of the source rises, an interplay between this and saturation of chemoreceptors gives rise to banding in *run-reverse* bacteria.

As a consequence of our model, we argue that while the volcano effect has so far not been observed, *run-reverse* bacteria exhibiting banding may provide a means to experimentally realize the volcano effect for the first time.

Materials and methods

Chemotaxis model

We consider bacterial motion as a general two-state process, consisting of a 'run' state—where a bacterium maintains its current direction—and a re-orientation characterized by an angle, ϕ, defining the change in direction between runs (i.e. the angular change from the direction of the current run to the direction of the next). *Run-reverse* and *run-and-tumble* are fundamentally distinguished from their angular re-orientation distributions as we discuss shortly.

We model our process in discrete time and, at every time step, the bacterium is assigned a probability, p, of continuing its run. Given the bacterium's current position, $\mathbf{r}_k$, its subsequent position, $\mathbf{r}_{k+1}$, is given by

$$\mathbf{r}_{k+1} = B(\mathbf{r}_k + \mathbf{v}_{run}\Delta t) + (1 - B)(\mathbf{r}_k + \mathbf{v}_{change}\Delta t) \tag{1}$$

where B is a Bernoulli random variable with parameter p, $B|p \sim Bern(p)$, and $\mathbf{v}_i$, with $i \in \{run, change\}$, is the bacterium's velocity. The direction of $\mathbf{v}_{run}$ is along a straight line from the previous to the current position and the direction of $\mathbf{v}_{change}$ is randomly sampled from the re-orientation anglular distribution (ϕ) as we discuss shortly. The run duration is the total time, sum over consecutive Δt's, for which the Bernoulli

random variable is sampled as 1. We parametrize our chemotaxis model presented in equation (1) based on the following observations:

(1) Bacteria are typically too small (as compared to eukaryotic cells) to measure spatial gradients directly across their body length. Instead they compare CA concentration changes in time as they move in space [12].

As a result, p—the probability of continuing a run from the bacterium's current position, r_k, to its subsequent position, r_{k+1} which we call the *p*-function—depends on the CA concentration at the bacterium's current and previous positions (r_k and r_{k-1}). The *p*-function is defined as follows

$$p(\mathbf{r}_{k+1}; \mathbf{r}_k, \mathbf{r}_{k-1}) = \alpha\left(\frac{c(\mathbf{r}_k)}{K + c(\mathbf{r}_k)} - \frac{c(\mathbf{r}_{k-1})}{K + c(\mathbf{r}_{k-1})}\right) + \beta. \tag{2}$$

Our minimal parameters capture: the proportionality between gradient and probability of run (α); the basal run probability in uniform CA concentrations (β); and saturation effects at high CA concentrations (K). In particular, we note that

$$\lim_{c \to 0} p = \beta.$$

Thus, in the absence of gradients, the bacterium reverts to a default probability $p = \beta$ of maintaining a run. An important note is in order: memory can often span multiple seconds in bacteria and we have investigated the effects of memory in previous work [5, 6]. The purpose of equation (2) is only to take the simplest of all models and show that it is sufficient to reproduce banding and the volcano effect as we will see shortly. Longer, and more experimentally realistic, memory

extending beyond that already incorporated in equation (2) would further exaggerate the features already exhibited by our model. What is more, a realistic memory would be parametrized from individual bacterial tracks using standard maximum likelihood tools that we have detailed in [5].

(2) Bacterial chemoreceptors saturate in regions of high CA. This is captured in our model at high CA concentration regions as follows

$$\lim_{c \to \infty} p = \beta.$$

This feature is a hallmark of bacterial adaptation [13, 14]. Furthermore, when $p = \beta$, the probability of maintaining a run is at a minimum (and, equivalently, the probability of re-orienting is at a maximum) which occurs in the absence of a gradient or in the presence of saturation.

(3) Bacteria spend longer in a 'run' state than a 're-orientation' state [15]. Coming back to the free parameters in our model, the α parameter rescales the values of the p-function to make sure its extrema are contained within $[0, 1]$. The p-function achieves its maximum near the point $\mathbf{r}$ along a given radial trajectory such that $c(\mathbf{r}) = K$. Therefore, the K parameter offers a handle on how far from the source the p-function can achieve its maximum. While our model provides a general framework, we mention that, in general, the parameter β is a probability that can be established experimentally from bacterial trajectories in uniform CA concentration profiles as we discussed in point 1 [5]. However, here we use a value for it from known tumbling probabilities.

(4) We consider the re-orientation angles to be normally distributed. That is $\phi | \mu, \sigma \sim N(\mu, \sigma)$, with mean μ and standard deviation σ. For example, *run-and-tumble* bacteria show a tumbling angle distribution with a mean of less than 90° in the presence of a CA gradient (i.e. a mean of 62° and a standard deviation of 26°, figure 3 in [10], for *E. coli*). However, angle re-orientation distributions for *run-reverse* motility exhibit a sharp peak at 180° associated with sharp reversals in addition to smaller peaks either at 0° associated with 'pauses' [9] (i.e. figure 1 in [16] for *Pseudomonas aeruginosa*) or alternatively at 90° associated with 'flicks' [17] (i.e. figure 2 in [18] for *Vibrio alginolyticus*).

(5) Finally, in order to parametrize the concentration dependence of the p-function to chemical stimuli, we consider a point food source, located at $\mathbf{r}_0$, from which CA particles are emitted with rate $\mathcal{R}$. CA particles then diffuse away from the source according to the following diffusion equation [5]

$$\frac{\partial c(\mathbf{r}, t)}{\partial t} = D\nabla^2 c(\mathbf{r}, t) - \frac{1}{\tau} c(\mathbf{r}, t) + \mathcal{R}\delta(\mathbf{r} - \mathbf{r}_0) \quad (3)$$

where D is the particle's diffusion coefficient, τ is the particle decay time constant, ∇^2 is the Laplacian and $\delta(...)$ the Dirac delta source term.

For a stationary CA source located at the origin, $\mathbf{r} = (0, 0, 0)$, the solution for the CA concentration is

$$c(\mathbf{r}, t) = \frac{\mathcal{R}}{4\pi D |\mathbf{r}|} e^{-\frac{|\mathbf{r}|}{\sqrt{D\tau}}}. \quad (4)$$

Implementing the chemotaxis model

To simulate bacterial trajectories near point sources, we first compute local concentrations at the bacterium's location based on the position of the point source. We then evaluate the corresponding p-function and, from this, probabilistically compute the bacterium's subsequent position. Typical simulated single bacterial trajectories are over 3000 time steps Δt with $\Delta t = 0.1$ s. We collect 1000 such trajectories to obtain statistics valid at the population level on all plots. The bacterial density in different regions of space around a CA source is computed by uniformly partitioning the domain into spherical shells centered at the source and counting the number of time steps (Δt) a bacterium falls on each shell (and normalizing by dividing each shell's density count by its volume).

Finally, we adjust the source's emission rate by simulating small point sources versus larger bead-like sources of CA. The diffusion constant (D) and the decay rate (τ)— fixed throughout this discussion— which characterize the size and stability of the CA molecules are, of course, independent of the source's emission rate (and thus effective size) of the source. To create bead-like sources reminiscent of experiments where marine bacteria exhibit banding near CA-soaked beads [3], we increase the emission rate such that the concentration near the source exceeds the saturation level of the bacterium and keep all other parameters fixed.

While our goal is to show that our model conclusions are robust over a broad and reasonable parameter range, we highlight, once again, that realistic models and model parameters (β, α, and K) may be inferred using maximum likelihood estimation (MLE) from cell tracking data in the presence of a simple linear CA gradient as has been demonstrated for a similar model in recent work [5]. In particular, uniform CA concentrations (i.e. no CA gradients) are sufficient to determine $\mathbf{v}_{run}$, μ, and σ from MLEs on experimental trajectories.

Results

Here we show that the experimentally motivated minimal model above captures banding, for the first time, and also predicts under what circumstances the volcano effect (theoretically predicted thus far and not observed) may be realized experimentally. While both volcano effect and banding might appear superficially
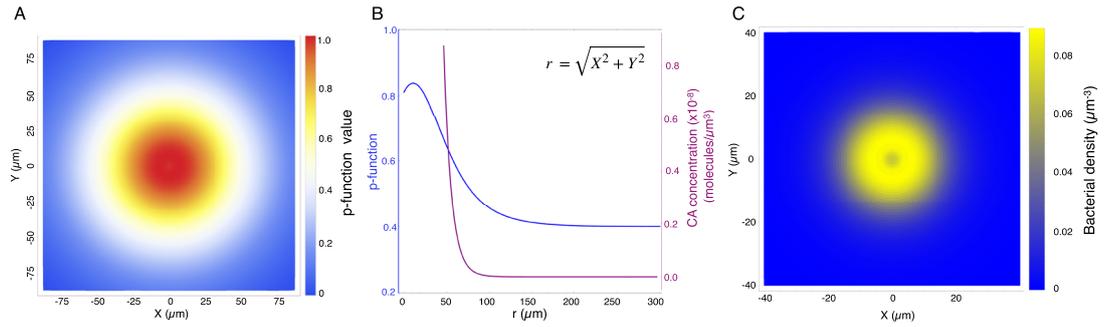
Figure 2. Bacteria exhibit the volcano effect around a point source of CA attributed to bacterial trajectories overshooting the point CA source. (A) A contour plot of the *p*-function produced by interpolating the value of the *p*-function at 100 000 uniformly distributed bacterial positions on the $(200.0 \ \mu m)^2 \ xy$-plane. (B) A combined plot of the *p*-function along a radial trajectory (left vertical axis) and the CA concentration (right vertical axis) versus radial distance from the point source. As we discuss in the main body, the *p*-function achieves its maximum near a point **r** such that $c(\mathbf{r}) = \mathbf{K}$, here $\mathbf{r} = 25.0 \ \mu m$. Away from that point, the *p*-function defaults to the β value. (C) A contour plot of the bacterial density—projected onto xy-plane—around the point CA source. This is plotted from a histogram of the normalized density of a population of 1000 bacteria over 3000 Δt time steps near the point source. The bins are comprised of 100 spherical shells of uniform thickness $\Delta r = 1.0 \ \mu m$. For all subplots here, we used $\beta = 0.4$, $\alpha = 2.9, K = 5.2 \times 10^{-5}$, and $| v_{run} | = 100.0 \ \mu m \, s^{-1}$ (typical swimming speeds in marine bacteria), and $| v_{change} | = 0.14 \ \mu m \, s^{-1}$ $(= \sqrt{D \times \Delta t}$, where $\Delta t = 0.1 \, s$ and D is a stationary bacterium's diffusion coefficient). Also, we used an emission rate of $\mathcal{R} = 200.0$ molecules s^{-1} for the point source and $[\phi | \mu, \sigma \sim N(\mu, \sigma) = N(165.0°, 5.0°)]$ for the angle change distribution. $\beta = 0.4$ is the default probability of tumbling in the absence of CA gradient. Most bacteria run for longer than they tumble [15], thereby justifying values of β below 0.5. A constraint on selecting α is to keep the *p*-function within $[0, 1]$ for a predetermined β and K while K determines the bacterium's saturation level. We use $K = 5.2 \times 10^{-5}$ in our simulation, based on an estimate for the concentration of amino acids in the location of a band [3].

similar (with bacteria concentrating at some distance from the source rather than on the source itself), we show that banding and the volcano effect arise as different limits of a simple chemotactic model.
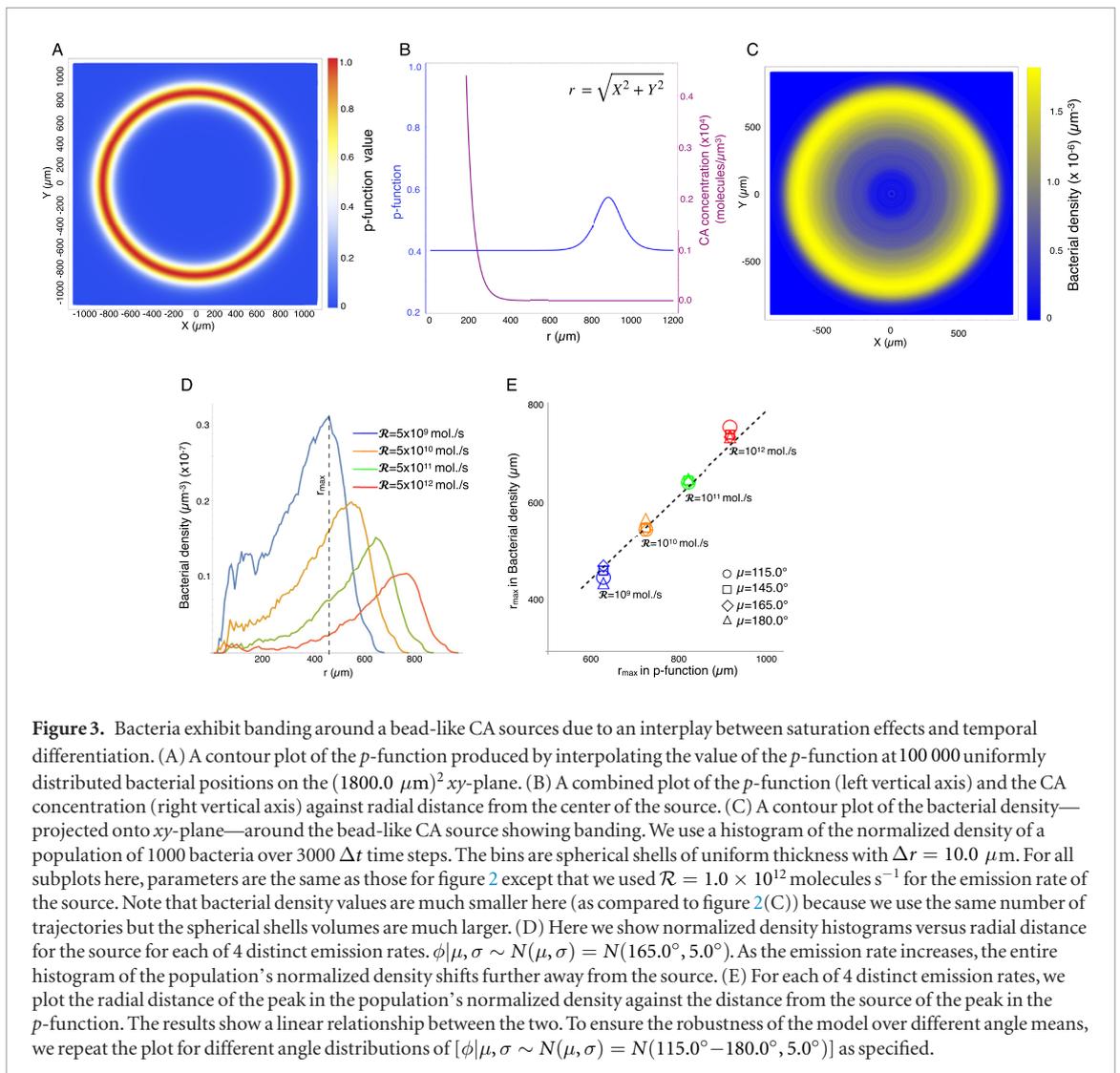
First, to recapitulate the volcano effect, we choose a low emission rate ($\mathcal{R}$) such that the CA concentration in space lies mostly below the foraging bacterium's saturation level. The results are shown in figure 2. Figure 2(A) shows a contour plot of the *p*-function— the probability of continuing a run—in the xy-plane as bacteria proceed toward the point source in a radial direction for values of parameters specified in the caption. Values of *p*-function are plotted against the radial distance from the point source in figure 2(B). The *p*-function peaks close to the point source (within a run length from the source). Provided the point of saturation (where the CA concentration exceeds K) is not far away from the point source, the bacterium experiences the sharp gradient near the source and therefore overshoots the point source through longer runs (as compared to those further away from the source). This probability drops to β (the default value) at radial distances far from the point CA source where the bacterium re-orients more often. As a result, bacteria spend most of their time in a shell-shaped region around, rather than on, the point source; see figure 2(C).

Having established that the minimal model presented reproduces the volcano effect, we now show that the very same model reproduces banding for different source emission rates (relevant to experiments with about 50.0 μm beads soaked with CA [3]). To mimic a large bead or food patch to which bacteria are attracted, we consider a point source of CA with very high emission rate such that the CA concentration in a much larger (compared to figure 2) spherical region

around the point source exceeds the saturation level; see figure 3.

Figure 3(A) shows a contour plot of the *p*-function over xy-plane as the bacterium swims toward the bead-like source. The *p*-function is plotted against the radial distance from the center of the bead-like source in figure 3(B). The *p*-function's peak is further away from the center of the source here as compared to figure 2. Similar to figure 2, the probability of continuing a run drops to the value assigned to β further away from the source. However, the *p*-function value also drops to the default value at smaller radial distances where the concentration of CA is higher than the saturation level. As a result, here we see banding behavior [3] for bacteria further away from the center of the bead-like source as compared to the case of a low emission point source where we observe a volcano effect (figure 2). Figure 3(C) shows a contour plot of population density of such bacteria around the source. In the region where the concentration of CA exceeds K, bacteria approaching the source acquire the (default) probability of running of β therefore tumbling more often and forming a band (figure 3(C)). This behavior is different than what was observed in figure 2 since the banding does not arise from overshooting the source as bacteria rarely venture into the region neighboring the source to begin with.

For figure 3, we looked at different emission rates in the range $\mathcal{R} = 1.0 \times 10^9 - 1.0 \times 10^{12}$ molecules s^{-1} (figure 3(D)). As expected by interpolating between both low and high emission regimes, the radial distance of the location with maximum bacterial density depends linearly on the maximum of the *p*-function (figure 3(E)). In addition, it is worth mentioning that for all results presented in this paper

Figure 3. Bacteria exhibit banding around a bead-like CA sources due to an interplay between saturation effects and temporal differentiation. (A) A contour plot of the *p*-function produced by interpolating the value of the *p*-function at 100 000 uniformly distributed bacterial positions on the $(1800.0\ \mu m)^2\ xy$-plane. (B) A combined plot of the *p*-function (left vertical axis) and the CA concentration (right vertical axis) against radial distance from the center of the source. (C) A contour plot of the bacterial density—projected onto *xy*-plane—around the bead-like CA source showing banding. We use a histogram of the normalized density of a population of 1000 bacteria over 3000 Δt time steps. The bins are spherical shells of uniform thickness with $\Delta r = 10.0\ \mu m$. For all subplots here, parameters are the same as those for figure 2 except that we used $\mathcal{R} = 1.0 \times 10^{12}$ molecules s^{-1} for the emission rate of the source. Note that bacterial density values are much smaller here (as compared to figure 2(C)) because we use the same number of trajectories but the spherical shells volumes are much larger. (D) Here we show normalized density histograms versus radial distance for the source for each of 4 distinct emission rates. $\phi | \mu, \sigma \sim N(\mu, \sigma) = N(165.0°, 5.0°)$. As the emission rate increases, the entire histogram of the population's normalized density shifts further away from the source. (E) For each of 4 distinct emission rates, we plot the radial distance of the peak in the population's normalized density against the distance from the source of the peak in the *p*-function. The results show a linear relationship between the two. To ensure the robustness of the model over different angle means, we repeat the plot for different angle distributions of $[\phi | \mu, \sigma \sim N(\mu, \sigma) = N(115.0° - 180.0°, 5.0°)]$ as specified.

we used $[\phi | \mu, \sigma \sim N(\mu, \sigma) = N(165.0°, 5.0°)]$ for angle re-orientation distributions meaning we employ a *run-reverse* swimming strategy. Our results are robust over turn angle distributions with mean range $\mu = 115.0 - 180.0°$ and constant $\sigma = 5.0°$ (figure 3(E)). We also performed analysis of our model for *run-and-tumble* motility ($\mu = 65.0 - 90.0°$ and $\sigma = 5.0°$) (data not shown). In summary, for low emission rates, we observe overshooting of bacteria and volcano effect for both *run-reverse* and *run-and-tumble* motilities. However, we only observe banding for *run-reverse* motility, not for the *run-and-tumble* motility. This is because random re-orientations (in *run-and-tumble*) as opposed to sharp reversals (in *run-reverse*) do not sufficiently re-direct bacteria away from the source. This may be the reason why banding is observed in marine bacteria with *run-reverse* motility but does not arise with *E. coli* that employs a *run-and-tumble* swimming strategy [3].

Discussion

Our model predicts the accumulation of bacteria around (rather than on) CA sources for small and large

CA sources for different physical reasons. Our model relies on effects such as temporal differentiation and saturation in bacterial response to CA sensing and does not contain signaling-level details. More specifically, our model predicts that the volcano effect and banding may both arise from the same model (and thus same bacterial species) but for different source emissions and that the, yet to be observed, volcano effect may be observed in bacteria that are already known to exhibit banding.

Beyond, signaling-level details there are other features that we have not incorporated into our model: (1) We assume constant run velocities. Yet *run-reverse* bacteria may employ 'flicks' as well which depend on the bacterium's swimming speed thereby enhancing chemotaxis by giving rise to faster climbing up CA gradients [17, 19]. Such effects, due to the compression of the hook at the flagellum's base, may contribute (and, in fact, enhance) banding. In principle, we can incorporate this effects by modifying equation (1). (2) We assume stationary sources. However, we may generalize our model to treat both moving point sources of food and turbulence in the medium in which the bacterium is foraging for food. The case of a moving source would be particularly relevant to marine bacteria such as *Pseudo-*

alteromonas haloplanktis and *Shewanella putrefaciens* known to sense and track individual free-swimming algae using *run-reverse* dynamics [4]. To make a source move, we may include a time dependent source $\mathbf{r}_0(t)$ in equation (3) based on the observable trajectory of the dynamical source. Furthermore, incorporating turbulence—by adding an advective term $\mathbf{u}(t) \cdot \nabla c(\mathbf{r}, t)$ to equation (3) where $\mathbf{u}(t) = (u_1(t), u_2(t), u_3(t))$ is the advective velocity—would be relevant to understanding the robustness of banding around CA sources in more complex environments [7].

Incorporating such effects would provide a quantitative, rather than qualitative, step forward toward understanding more species-specific band structures of marine bacteria such as *P. haloplanktis*, *S. putrefaciens*, and *Deleya marina* and the degree of interaction between individual bacteria and copepods (figure 4 in [17]), lysed ciliates [20] or even bacterial clusters [21].

AQ3

Acknowledgments

AQ4

ORCID iDs

AQ5

Steve Pressé   https://orcid.org/0000-0002-5408-0718

References

AQ6

AQ7

[1] Eisenbach M 2004 *Chemotaxis* (Imperial College Press)
[2] Berg H C 2004 *E. Coli in Motion* (Berlin: Springer)
[3] Barbara G M and Mitchell J G 2003 Marine bacterial organisation around point-like sources of amino acids *FEMS Microbiol. Ecol.* **43** 99

[4] Barbara G and Mitchell J 2003 Bacterial tracking of motile algae *FEMS Microbiol. Ecol.* **44** 79
[5] Jashnsaz H, Nguyen T, Petrache H I and Pressé S 2015 Inferring models of bacterial dynamics toward point sources *PLoS One* **10** e0140428
[6] Jashnsaz H, Anderson G G and Pressé S 2017 Statistical signatures of a targeted search by bacteria *Phys. Biol.* https://doi.org/10.1088/1478-3975/aa84e AQ8
[7] Luchsinger R H, Bergersen B and Mitchell J G 1999 Bacterial swimming strategies and turbulence *Biophys. J.* **77** 2377–86
[8] Jashnsaz H *et al* 2017 Hydrodynamic hunters *Biophys. J.* **112** 1282–9
[9] Bray D, Levin M D and Lipkow K 2007 The chemotactic behavior of computer-based surrogate bacteria *Curr. Biol.* **17** 12
[10] Segall J E, Block S M and Berg H C 1986 Temporal comparisons in bacterial chemotaxis *Proc. Natl Acad. Sci. USA* **83** 8987
[11] Macnab R M and Koshland D E 1972 The gradient-sensing mechanism in bacterial chemotaxis *Proc. Natl Acad. Sci. USA* **69** 2509–12
[12] Tu Y 2013 Quantitative modeling of bacterial chemotaxis: signal amplification and accurate adaptation *Annu. Rev. Biophys.* **42** 337
[13] Saragosti J, Silberzan P and Buguin A 2012 Modeling *E. coli* tumbles by rotational diffusion; implications for chemotaxis *PLoS One* **7** 35412
[14] Berg H C and Brown D A 1972 Chemotaxis in *Escherichia coli* analysed by three-dimensional tracking *Nature* **239** 500
[15] Qian C, Wong C C, Swarup S and Chiam K H 2013 Bacterial tethering analysis reveals a run-reverse-turn mechanism for pseudomonas species motility *Appl. Environ. Microbiol.* **79** 4734–43
[16] Cai Q, Li Z, Ouyang Q, Luo C and Gordon V D 2016 Singly flagellated pseudomonas aeruginosa chemotaxes efficiently by unbiased motor regulation *mBio* **7** e00013–16
[17] Son K, Guasto J S and Stocker R 2013 Bacteria can exploit a flagellar buckling instability to change direction *Nat. Phys.* **9** 494–8
[18] Xie L, Altindal T, Chattopadhyay S and Wu X L 2011 Bacterial flagellum as a propeller and as a rudder for efficient chemotaxis *Proc. Natl Acad. Sci.* **108** 2246–51
[19] Son K, Menolascina F and Stocker R 2016 Speed-dependent chemotactic precision in marine bacteria *Proc. Natl Acad. Sci. USA* **113** 8624–9
[20] Blackburn N, Fenchel T and Mitchell J 1998 Microscale nutrient patches in planktonic habitats shown by chemotactic bacteria *Science* **282** 2254
[21] Mittal N, Budrene E O, Brenner M P and Oudenaarden A V 2003 Motility of Escherichia coli cells in clusters formed by chemotactic aggregation *Proc. Natl Acad. Sci. USA* **100** 13259–63